1521-0111/94/3/973–983$35.00
MOLECULAR PHARMACOLOGY

https://doi.org/10.1124/mol.118.112441
Mol Pharmacol 94:973–983, September 2018

Molecular Determinants of the Differential Modulation of $Ca_V1.2$ and $Ca_V1.3$ by Nifedipine and FPL 64176[S]

Yuchen Wang,[1] Shiqi Tang,[1] Kyle E. Harvey, Amy E. Salyer, T. August Li, Emily K. Rantz, Markus A. Lill, and Gregory H. Hockerman

Department of Medicinal Chemistry and Molecular Pharmacology, Purdue University College of Pharmacy, West Lafayette, Indiana

Received March 9, 2018; accepted June 28, 2018

ABSTRACT

Nifedipine and FPL 64176 (FPL), which block and potentiate L-type voltage-gated Ca^{2+} channels, respectively, modulate $Ca_V1.2$ more potently than $Ca_V1.3$. To identify potential strategies for developing subtype-selective inhibitors, we investigated the role of divergent amino acid residues in transmembrane domains IIIS5 and the extracellular IIIS5-3P loop region in modulation of these channels by nifedipine and FPL. Insertion of the extracellular IIIS5-3P loop from $Ca_V1.2$ into $Ca_V1.3$ ($Ca_V1.3+$) reduced the IC_{50} of nifedipine from 289 to 101 nM, and substitution of S1100 with an A residue, as in $Ca_V1.2$, accounted for this difference. Substituting M1030 in IIIS5 to V in $Ca_V1.3+$ ($Ca_V1.3+V$) further reduced the IC_{50} of nifedipine to 42 nM. FPL increased current amplitude with an EC_{50} of 854 nM in $Ca_V1.3$, 103 nM in $Ca_V1.2$, and 99 nM in $Ca_V1.3+V$. In contrast to nifedipine block, substitution of M1030 to V in $Ca_V1.3$ had no effect on potency of FPL potentiation of current amplitude, but slowed deactivation in the presence and absence of 10 μM FPL. FPL had no effect on deactivation of $Ca_V1.3$/dihydropyridine-insensitive (DHPi), a channel with very low sensitivity to nifedipine block (IC_{50} ~93 μM), but did shift the voltage-dependence of activation by ~−10 mV. We conclude that the M/V variation in IIIS5 and the S/A variation in the IIIS5-3P loop of $Ca_V1.2$ and $Ca_V1.3$ largely determine the difference in nifedipine potency between these two channels, but the difference in FPL potency is determined by divergent amino acids in the IIIS5-3P loop.

Introduction

Inhibitors of L-type voltage-gated Ca^{2+} channels have long been used in the treatment of cardiovascular diseases such as hypertension and angina pectoris. In these indications, the specific target is inhibition of $Ca_V1.2$, the predominant L-type channel in vascular smooth muscle, to induce vasodilation (Catterall, 2000). However, the closely related L-type channel $Ca_V1.3$ is expressed in SA and AV nodal tissue (Platzer et al., 2000), and is probably an important target for suppression of supraventricular arrhythmias. None of the three chemical classes of L-type channels blockers currently in clinical use [dihydropyridines (DHPs), phenylalkylamines (PAAs), or benzothiazepines (BTZs) (Hockerman et al., 1997b)] have a high degree of discrimination between $Ca_V1.2$ and $Ca_V1.3$. Outside of the cardiovascular system, $Ca_V1.2$ and $Ca_V1.3$ are expressed in various types of neurons (Hell et al., 1993) and endocrine cells (Seino et al., 1992), where they are thought to play distinct roles in cellular regulation. For example, $Ca_V1.3$ has been implicated in mediating Ca^{2+} oscillations in dopaminergic neurons of the substantia nigra that may lead to Ca^{2+} overload and contribute to the selective loss of these neurons in Parkinson's disease (Guzman et al., 2009, 2010; Surmeier and Schumacker, 2013). In addition, autoantibodies that activate $Ca_V1.3$ have been detected in serum from patients with type 1 diabetes (Juntti-Berggren et al., 1993; Bason et al., 2013), suggesting a role for excessive $Ca_V1.3$ activation in autoimmune-mediated β cell death. These observations have driven the search for selective inhibitors of $Ca_V1.3$ as potential therapeutics for Parkinson disease and type 1 diabetes.

Given the attractiveness of $Ca_V1.3$ as therapeutic targets, several efforts to develop subtype-selective L-type channel blockers have been published. One study examined dozens of derivatives of the DHP scaffold but reported only modest degrees of selectivity for $Ca_V1.3$ over $Ca_V1.2$ (Chang et al., 2010), and another study examining 5-unsubstituted DHPs reported compounds with better $Ca_V1.3$ selectivity (Tenti et al., 2014). A screen of over 60,000 compounds identified a class of compounds, pyrimidine-2,4,6-triones, as moderately selective inhibitors of $Ca_V1.3$ over $Ca_V1.2$ (Kang et al., 2012, 2013). However, one follow-up study concluded that the selectivity of the lead pyrimidine-2,4,6-trione (compound 8)

This work was supported by a grant from the American Heart Association Midwest Affiliate [15GRNT25750021] to G.H.H.
[1]Y.W. and S.T. contributed equally to this work.
https://doi.org/10.1124/mol.118.112441.
[S] This article has supplemental material available at molpharm.aspetjournals.org.

ABBREVIATIONS: Bay K 8644, methyl 2,6-dimethyl-5-nitro-4-[2-(trifluoromethyl)phenyl]-1,4-dihydropyridine-3-carboxylate; BTZ, benzothiazepines; DHP, dihydropyridines; FPL 64176, 2,5-dimethyl-4-[2-(phenylmethyl)benzoyl]-1*H*-pyrrole-3-carboxylic acid methyl ester; HEPES, 4-(2-hydroxyethyl)piperazine-1-ethanesulfonic acid; nifedipine, 1,4-dihydro-2,6-dimethyl-4-(2-nitrophenyl)-3,5-pyridinecarboxylic acid dimethyl ester; NMDG, *N*-methyl-D-glucamine; PAA, phenylalkylamine.

was dependent on the subtype of the auxiliary β subunit expressed with $Ca_v1.3$ (Huang et al., 2014), and another concluded that compound 8 was an activator of L-type channels (Ortner et al., 2014).

The mixed results reported in studies using derivatives of DHPs or screens of chemical libraries suggest the need for more insight into differences between $Ca_v1.2$ and $Ca_v1.3$ that might be exploited in selective-drug development. The molecular pharmacology of $Ca_v1.2$ is well studied. The molecular determinants of $Ca_v1.2$ modulation by DHPs (Hockerman et al., 1997c; Sinnegger et al., 1997; Yamaguchi et al., 2003; Lin et al., 2011), PAAs (Hockerman et al., 1995, 1997a; Dilmac et al., 2004), and BTZs (Hering et al., 1996; Hockerman et al., 2000; Dilmac et al., 2003) have been identified, and homology models of the binding sites have been developed (Cosconati et al., 2007; Cheng et al., 2009; Tikhonov and Zhorov, 2009). On the other hand, the molecular pharmacology of $Ca_v1.3$ has not been extensively studied. One reason for this disparity may be that the critical residues for drug block of $Ca_v1.2$ are highly conserved in $Ca_v1.3$, leading to the perception that the drug binding site in both channels is identical. However, $Ca_v1.3$ is reported to be less sensitive to block by some DHPs than $Ca_v1.2$ (Xu and Lipscombe, 2001; Huang et al., 2013), but the molecular determinants that mediate this difference in DHP affinity are not known.

The transmembrane domains of $Ca_v1.2$ and $Ca_v1.3$ that compose the drug binding pockets are nearly identical, but two subtle differences, one each in IIIS5 and IIIS6, exist. In addition, the extracellular IIIS5-3P domains of these channels are highly divergent. The IIIS5-3P domain contains two amino acid residues that are critical for DHP block of $Ca_v1.2$ (Yamaguchi et al., 2000, 2003), yet these residues are conserved between $Ca_v1.2$ and $Ca_v1.3$. However, another cluster of amino acids, closer to IIIS5 and not conserved between $Ca_v1.2$ and $Ca_v1.3$ is reported to influence DHP binding affinity (Wang et al., 2007). Therefore, we examined if substitution of these key divergent amino acids from $Ca_v1.2$ into $Ca_v1.3$ could reduce the IC_{50} for nifedipine (1,4-dihydro-2,6-dimethyl-4-(2-nitrophenyl)-3,5-pyridinecarboxylic acid dimethyl ester) and EC_{50} for the L-type channel agonist FPL 64176 compared with wild-type $Ca_v1.3$.

Materials and Methods

Chemicals and Reagents. All reagents, unless otherwise indicated, were purchased from MilliporeSigma (St. Louis, MO). Oligonucleotides used for site-directed mutagenesis were obtained from GenScript (Nanjing, People's Republic of China). The $Ca_v1.3_{42}$ (AF370010) and $Ca_v1.3_{42a}$ (AF370009) clones (Xu and Lipscombe, 2001) with three cloning errors repaired (Huang et al., 2013) were the gift of Dr. Tuk-Wah Soong, University of Singapore. The $Ca_v1.2$ clone (M67515) (Snutch et al., 1991) was the gift of Dr. Terrance Snutch, University of British Columbia.

Cell Culture. The tsA201 variant of the human embryonic kidney 293 cell line was grown at 37°C, 5% CO_2, in Dulbecco's modified Eagle's medium (Life Technologies/Thermo Fisher Scientific, Grand Island, NY) supplemented with 10% fetal bovine serum (Atlanta Biologic, Lawrenceville, GA), 100 IU/ml penicillin, and 100 μg/ml streptomycin.

Site-Directed Mutagenesis. All mutant $Ca_v1.3_{42}$ (in pcDNA6) and $Ca_v1.2$ (in pcDNA3) α_1 subunits (except $Ca_v1.3+$) were constructed as described previously (Dilmac et al., 2003). To construct $Ca_v1.3+$, an oligonucleotide encoding amino acids 1058–1118 of $Ca_v1.2$ was ligated into $Ca_v1.3_{42}$ in pSPORT6 after excision of the IIIS5-3P encoding DNA with BamH1 and BstB1. The final version in $Ca_v1.3_{42}$ pcDNA6 was created by ligation of the BamH1/EcoRV fragment containing the chimeric region from pSPORT6. All mutant constructs were verified by DNA sequencing and restriction digest analysis.

Electrophysiological Recordings. Mutant and wild type $Ca_v1.2$ or $Ca_v1.3$ α_1 subunits were coexpressed with $\alpha_2\delta_1$ (Williams et al., 1992) and β_3 (Castellano et al., 1993) subunits (both in pcDNA3), and pEGFPN1 (Clontech, Mountain View, CA) by transfection of tsA201 cells, as described previously (Dilmac et al., 2003). Transfected cells were identified by green fluorescent protein fluorescence. Micropipettes were pulled from borosilicate capillaries to an inside diameter of approximately 3–5 μm using a Sutter P-87 pipette puller (Sutter Instruments, Novato, CA), and polished with a Narishige MF 830 micro forge (Narishige, Amityville, NY). The pipette solution contained: (in millimolars) 180 NMDG, 40 HEPES, 4 $MgCl_2$, 12 phosphocreatine, 5 BAPTA, 2 Na_2ATP, 0.5 Na_3GTP, 0.1 leupeptin, and pH was adjusted to 7.3. The extracellular solution contained (in millimolars): 140 NaCl, 20 $CsCl_2$, 10 $BaCl_2$, 10 HEPES, 10 glucose, 10 sucrose, 1 $MgCl_2$, and pH was adjusted to 7.4. In experiments with balanced NMDG, the extracellular solution was altered to contain 30 mM NMDG, with a corresponding reduction in NaCl concentration. Whole-cell voltage clamp recordings were made at room temperature using an Axopatch 200B amplifier (Axon Instrument, Sunnyvale, CA). Data were sampled at 10 kHz and filtered at 1 kHz. Drugs were applied in the extracellular solution with a Biologic RSC 160 perfusion system (BioLogic, Sayssinet-Pariset, France). $logIC_{50}$ values for nifedipine block were determined by fitting the fraction of current blocked at each drug concentration to the equation: Fraction Blocked = a − (a/(1 + ([nifedipine]/IC_{50})^b)), where a = maximum fraction blocked, b = slope. $logEC_{50}$ values for FPL potentiation were determined by normalizing the increase in current with each concentration of FPL to the increase in current observed with 10 μM FPL. When fitting equations to the nifedipine dose-response data ($logIC_{50}$), we set the minimum at zero, and let the slope and maximal block vary. This reflects the experimental observation that current block is often incomplete even at maximally effective concentrations. When fitting equations to the FPL 64176 dose-response data ($logEC_{50}$), we set the minimum at zero and the maximum at 1 (maximal current stimulation) but allowed slope to vary. The range of N values for dose-response curves represent the number of data points for each drug concentration. The number of separate experiments performed (i.e., cells clamped) to obtain a given dose-response curve is equal to or greater than the highest number of replicates indicated for any single drug concentration. The basis of the $logIC_{50}$ and $logEC_{50}$ values ± S.E. of the fit shown in Table 1 is the fit of all of the data for a given channel construct. $V_{1/2}$ activation values were determined by plotting normalized tail-current amplitudes versus the corresponding 100-millisecond depolarizing voltage steps from −50 to +60 mV, in 10 mV-increments, from a holding potential of −80 mV. The data were fit to the equation, $I = 1/(1 + exp((V_{1/2} - V)/k))$, where k is a slope factor. The steady-state inactivation protocol used 10-second conditioning pulses from −80 to +20 mV in 10-mV increments from a holding potential of −90 mV, followed by a 100-millisecond test pulse to +10 mV. $V_{1/2}$ inactivation was determined by plotting the normalized test pulse amplitude versus the conditioning pulse potential, and fitting the data to the equation $I = 1/(1 + exp(-(V - V_{1/2})/k))$, where k is a slope factor. When fitting equations to the data for voltage-dependence of activation and inactivation, we set curves to start at 0 or 1, respectively, and force the curves to plateau at 1 or 0, respectively. Slopes were allowed to vary. The time course of channel deactivation was determined by fitting tail-current decay to either a single or double exponential function.

Homology Models of $Ca_v1.2$ and $Ca_v1.3$ on the Basis of the Structure of $Ca_v1.1$. Homology models of $Ca_v1.2$ and $Ca_v1.3$ were generated using SWISS-MODEL (Guex et al., 2009; Benkert et al., 2011; Bertoni et al., 2017; Bienert et al., 2017; Waterhouse et al., 2018).

TABLE 1
Pharmacology and voltage-dependence of $Ca_v1.2$, $Ca_v1.3$, and mutant channels

Channel (+ β_3 & $\alpha_2\delta_1$)	Nifedipine Log IC_{50}	Nifedipine Hill Slope	Nifedipine Max	FPL64176 Log EC_{50}	$V_{1/2}$inact.	$V_{1/2}$act.	$\Delta V_{1/2}$act. FPL
			%		*mV*	*mV*	*mV*
$Ca_v1.2$	−7.59 ± 0.03 *N* = 3–12	1.0 ± 0.1	90 ± 3	−6.95 ± 0.16 *N* = 3–8	−41 ± 0.6 *N* = 6	−20 ± 0.5 *N* = 6	−26 ± 0.7 *N* = 7
$Ca_v1.3$ (long)	−6.54 ± 0.04 *N* = 7	0.78 ± 0.05	88 ± 2	−6.05 ± 0.08[a] *N* = 3–7	−36 ± 1.3 *N* = 5	−30 ± 1.5 *N* = 9	−10.2 ± 1.8 *N* = 9
$Ca_v1.3$ 42a (short)	−6.36 ± 0.02 *N* = 5 to 6	1.0 ± 0.05	91 ± 2	ND	−40 ± 1.2 *N* = 5	−28 ± 0.7 *N* = 5	ND
$Ca_v1.3$/DHPi	~ −4.0 *N* = 2–16	ND	ND	ND	−27 ± 1.2 *N* = 5	−22 ± 1.1 *N* = 9	−9.5 ± 1.4 *N* = 6
$Ca_v1.3$/MV	−7.05 ± 0.04 *N* = 5–7	1.3 ± 0.15	81 ± 2	−6.97 ± 0.05 *N* = 3–7	−35 ± 0.5 *N* = 6	−26 ± 1.1 *N* = 23	ND
$Ca_v1.2$/VM	−7.41 ± 0.07 *N* = 4–6	0.83 ± 0.11	94 ± 4	ND	−38 ± 0.5 *N* = 6	−24 ± 1.0 *N* = 8	ND
$Ca_v1.3$+	−7.00 ± 0.02 *N* = 6–8	0.79 ± 0.02	87 ± 1	ND	−38 ± 1.6 *N* = 7	−29 ± 0.8 *N* = 12	ND
$Ca_v1.3$+V	−7.37 ± 0.05 *N* = 4–10	1.4 ± 0.16	83 ± 2	−6.97 ± 0.05 *N* = 3–7	−42 ± 0.3 *N* = 4	−28 ± 1.2 *N* = 8	−8.2 ± 1.8 *N* = 7
$Ca_v1.3$/PEEP	−6.73 ± 0.07 *N* = 3–7	0.43 ± 0.02	80 ± 2	−5.93 ± 0.03 *N* = 4 to 5	−36 ± 0.2 *N* = 3	−27 ± 0.8 *N* = 6	ND
$Ca_v1.3$/N6	−6.93 ± 0.20[a] *N* = 5–9	0.52 ± 0.12	66 ± 5	−6.05 ± 0.15[a] *N* = 8–12	−34 ± 0.6 *N* = 5	−17 ± 0.8 *N* = 9	ND
$Ca_v1.3$/SA	−7.01 ± 0.11 *N* = 4 to 5	0.82 ± 0.2	90 ± 5	−6.01 ± 0.40 *N* = 3–18	−49 ± 0.8 *N* = 12	−29 ± 1.5 *N* = 12	ND

ND, Not determined.
[a]Data collected using balanced NMDG solutions.

The structure of $Ca_v1.1$ (PDB-code: 5gjw) was used as template for modeling (Wu et al., 2016). $Ca_v1.2$ and $Ca_v1.3$ share sequence identities of 72% and 71% with $Ca_v1.1$, respectively.

Data Analysis and Statistics. Data were analyzed using Clampfit 10.6 (Axon Instruments) and SigmaPlot 11 (Systat Software, San Jose, CA). logIC_{50} and logEC_{50} values were determined using GraphPad Prism 7.04 (GraphPad Software, La Jolla, CA). Comparisons of two means were made with Student's unpaired *t* test. Comparisons of three or more means were made using one-way analysis of variance. $P < 0.05$ was considered significant. Data shown are means ± S.E. Lines are fits of the equations indicated for each type of experiment to the data.

Results

Characterization of Ba^{2+} Current Conducted by $Ca_v1.2$ or $Ca_v1.3$ Coexpressed with the β_3 and $\alpha_2\delta_1$ Subunits in tsA201 Cells. We assessed the biophysical and pharmacological properties of $Ca_v1.2$ and $Ca_v1.3$ in our expression system. As expected, $Ca_v1.3$ activated at more negative voltages than $Ca_v1.2$ ($P < 0.001$) (Fig. 1A; Table 1), and $Ca_v1.2$ inactivated at slightly more negative voltages than $Ca_v1.3$ ($P < 0.01$) (Fig. 1B; Table 1). We next examined the potency of nifedipine block of both channel types. We chose nifedipine because it is the most compact of the dihydropyridine Ca^{2+} channel antagonists (Supplemental Fig. 1), and our preliminary screen of several structurally distinct dihydropyridines revealed a substantial difference in nifedipine potency in blocking $Ca_v1.2$ compared with $Ca_v1.3$ (Supplemental Fig. 1). Channels were activated with 100-millisecond steps to +10 mV at a frequency of 0.033 Hz from a holding potential of −80 mV. After a baseline current was established, increasing concentrations of nifedipine were applied via a perfusion capillary in the bath solution. Figure 1C shows sample traces and the compiled dose-response curves for both channel subtypes. As expected, $Ca_v1.2$ was blocked more potently by nifedipine than $Ca_v1.3$, with IC_{50} values of 22 ± 2 nM and 289 ± 30 nM, respectively ($P < 0.001$). The truncated splice variant $Ca_v1.3_{42a}$ (Xu and Lipscombe, 2001) had been reported to be less sensitive to nifedipine than the full-length $Ca_v1.3_{42}$ variant (Huang et al., 2013). Therefore, we examined the dose-dependence of nifedipine block of $Ca_v1.3_{42a}$, and determined the IC_{50} for nifedipine to be 436 ± 24 nM, greater than that of $Ca_v1.3_{42}$ ($P < 0.01$) (Fig. 1C). We chose to use the full-length $Ca_v1.3_{42}$ variant in the subsequent experiments, since it is structurally more similar to the $Ca_v1.2$ variant used in this study.

The IIIS5 Transmembrane Domain Plays a Key Role in Nifedipine Block of $Ca_v1.3$. Studies in $Ca_v1.2$ have established transmembrane domain IIIS5 as a key component of the DHP binding pocket (Mitterdorfer et al., 1996). Specifically, mutations of T1039 and Q1043 (underlined in Fig. 2A) to the corresponding residues in DHP-insensitive voltage-gated Ca^{2+} channels results in a $Ca_v1.2$ mutant channel (termed $Ca_v1.2$/DHPi) that is markedly less sensitive to DHPs but normally sensitive to diltiazem (Hockerman et al., 2000; Lin et al., 2011). We made the corresponding $Ca_v1.3$/DHPi mutant, and as expected, it was substantially less sensitive to nifedipine than $Ca_v1.3$ (Fig. 2B). In fact, we were unable to determine the maximum percent of $Ca_v1.3$/DHPi current blocked because the nifedipine concentrations at the high end of the range (>200 μM) were at the limit of aqueous solubility (Ran et al., 2002). Assuming maximal inhibition of 90% of current, we estimated the IC_{50} of nifedipine block of $Ca_v1.3$/DHPi to be ~93 μM, more than 300 times that for $Ca_v1.3$. As with the corresponding mutation in $Ca_v1.2$ (Hockerman et al., 2000), the sensitivity of $Ca_v1.3$/DHPi to block by the BTZ diltiazem was not reduced compared with $Ca_v1.3$ (Supplemental Fig. 2).

Given that transmembrane domain IIIS5 clearly contributes to the DHP binding pocket in $Ca_v1.3$, we next examined the single amino acid in this domain that is not conserved between $Ca_v1.2$ and $Ca_v1.3$, M1030 (Fig. 2A). The corresponding position

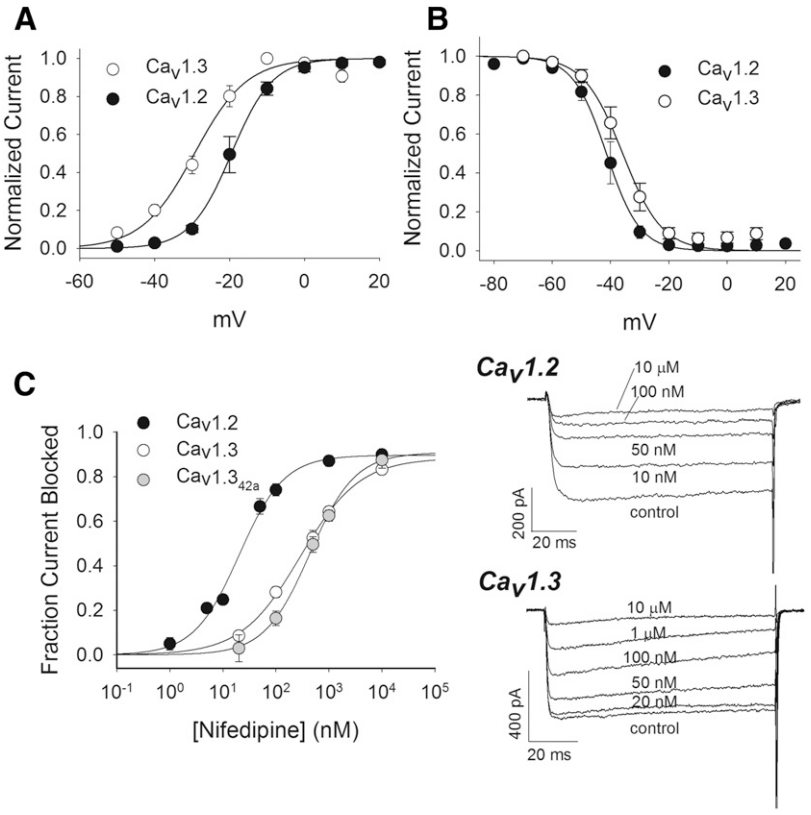

Fig. 1. Characterization of $Ca_v1.2$ and $Ca_v1.3$ biophysical properties and nifedipine block. (A) Determination of the voltage-dependence of activation in $Ca_v1.2$ and $Ca_v1.3$. $V_{1/2}$ activation values were -20 ± 0.5 mV for $Ca_v1.2$ ($N = 6$) and -30 ± 1.5 mV for $Ca_v1.3$ ($N = 9$) ($P < 0.001$). (B) Determination of the voltage-dependence of inactivation in $Ca_v1.2$ and $Ca_v1.3$. $V_{1/2}$ inactivation values were -41 ± 0.6 mV for $Ca_v1.2$ ($N = 6$) and -36 ± 1.3 mV ($N = 5$) for $Ca_v1.3$ ($P < 0.01$). (C) Determination of potency of nifedipine block of $Ca_v1.2$ and $Ca_v1.3$. The IC_{50} values of nifedipine block were 22 ± 2 nM ($N = 3$–12) for $Ca_v1.2$ and 289 ± 30 nM ($N = 7$) for $Ca_v1.3$ ($P < 0.001$). Example traces from experiments are shown at right. The IC_{50} for nifedipine block of $Ca_v1.3_{42a}$, a truncated splice variant, was 436 ± 24 nM ($N = 5$ to 6), statistically significantly greater than that of $Ca_v1.3$ ($P < 0.01$).

in $Ca_v1.2$ (1036) is occupied by a V residue, so we constructed the mutant channel $Ca_v1.3$/MV, to determine if this conservative change could contribute to the difference in nifedipine potency between $Ca_v1.2$ and $Ca_v1.3$. The $V_{1/2}$ inactivation of $Ca_v1.3$/MV was not different from that of $Ca_v1.3$; however, the $V_{1/2}$ activation of $Ca_v1.3$/MV (-26 ± 1.1) (Table 1) was more positive than that for $Ca_v1.3$ ($P < 0.05$). The M1030V mutation increased the potency of nifedipine block of $Ca_v1.3$, reducing the IC_{50} from 289 to 89 ± 7 nM ($P < 0.001$) (Fig. 2C). Given that this relatively conservative change in structure shifted the potency of nifedipine block of $Ca_v1.3$ toward those of $Ca_v1.2$, we asked if the reciprocal change in $Ca_v1.2$ ($Ca_v1.2$/VM) would shift the potency of nifedipine block toward that of $Ca_v1.3$. Indeed, we found that the V1036M mutation increased the IC_{50} of nifedipine for block of current compared with $Ca_v1.2$ (39 ± 6 nM) ($P < 0.05$) (Fig. 2D). In addition, the $V_{1/2}$ activation of $Ca_v1.2$/VM was -24 ± 1 mV, more negative than that for $Ca_v1.2$ ($P < 0.01$) (Fig. 2E; Table 1). Thus, this single, conservative difference between $Ca_v1.2$ and $Ca_v1.3$ in transmembrane segment IIIS5 contributes to differences in both voltage-dependence of activation and nifedipine potency between these two channels.

The Extracellular Domain IIIS5-3P Contributes to the Difference in Nifedipine Potency Between $Ca_v1.2$ and $Ca_v1.3$. Given that the small difference in amino acid sequence between $Ca_v1.2$ and $Ca_v1.3$ in IIIS5 only partially accounts for the difference in nifedipine potency, we next examined the role of the extracellular domain just downstream of IIIS5, the IIIS5-3P loop. This region is an area of relatively high amino acid sequence divergence between $Ca_v1.2$ and $Ca_v1.3$ (Fig. 3A), and some determinants of DHP potency/affinity have been identified in this region. Therefore, we created a chimeric channel, $Ca_v1.3+$ that incorporates the $Ca_v1.2$ IIIS5-3P loop into the $Ca_v1.3$ background, to determine the effect of this region on the potency of nifedipine block. The voltage-dependence of activation and inactivation were both essentially unchanged in $Ca_v1.3+$ compared with $Ca_v1.3$ (see Table 1). However, the IC_{50} for nifedipine block of $Ca_v1.3+$ (101 ± 4 nM) was reduced compared with that for $Ca_v1.3$ ($P < 0.001$) (Fig. 3B).

We next asked if a particular region of the IIIS5-3P loop could account for the increase in nifedipine potency in block of $Ca_v1.3+$ versus $Ca_v1.3$. The IIIS5-3P loop extends from the end of IIIS5 to the conserved E residue in the domain III selectivity filter (Fig. 3A). The region just upstream of the conserved selectivity filter E residue of homologous domain IIII (Yang et al., 1993) (1118 in $Ca_v1.2$, 1112 in $Ca_v1.3$; Fig. 3A) is known to be involved in DHP modulation of $Ca_v1.2$ (Yamaguchi et al., 2000, 2003) but is highly conserved between $Ca_v1.2$ and $Ca_v1.3$. Mutation of the nearest nonconserved residue upstream of E1112 in $Ca_v1.3$ (S1100) resulted in a channel ($Ca_v1.3$/SA) with $V_{1/2}$ activation not different from $Ca_v1.3$ but with markedly left-shifted $V_{1/2}$ inactivation (see Table 1). The IC_{50} for nifedipine block of $Ca_v1.3$/SA was 99 ± 24 nM, indistinguishable from that for $Ca_v1.3+$ (Fig. 3B). The IIIS5-3P loop of both $Ca_v1.2$ and $Ca_v1.3$ contain two P residues, one of which is conserved (1081/1087) and another that differs significantly in position relative to the conserved P residue (P1063 in $Ca_v1.3$ and P1091 in $Ca_v1.2$) (see Fig. 3A). We reasoned that this difference in P configuration could affect the conformation of the conserved, distal portion of the IIIS5-3P loop, and thus DHP affinity. Therefore, we created $Ca_v1.3$/PEEP, with P residues at position 1081 and 1085, but a P to E switch at position 1063, mimicking the P configuration of the $Ca_v1.2$ IIIS5-3P loop. The voltage-dependence of

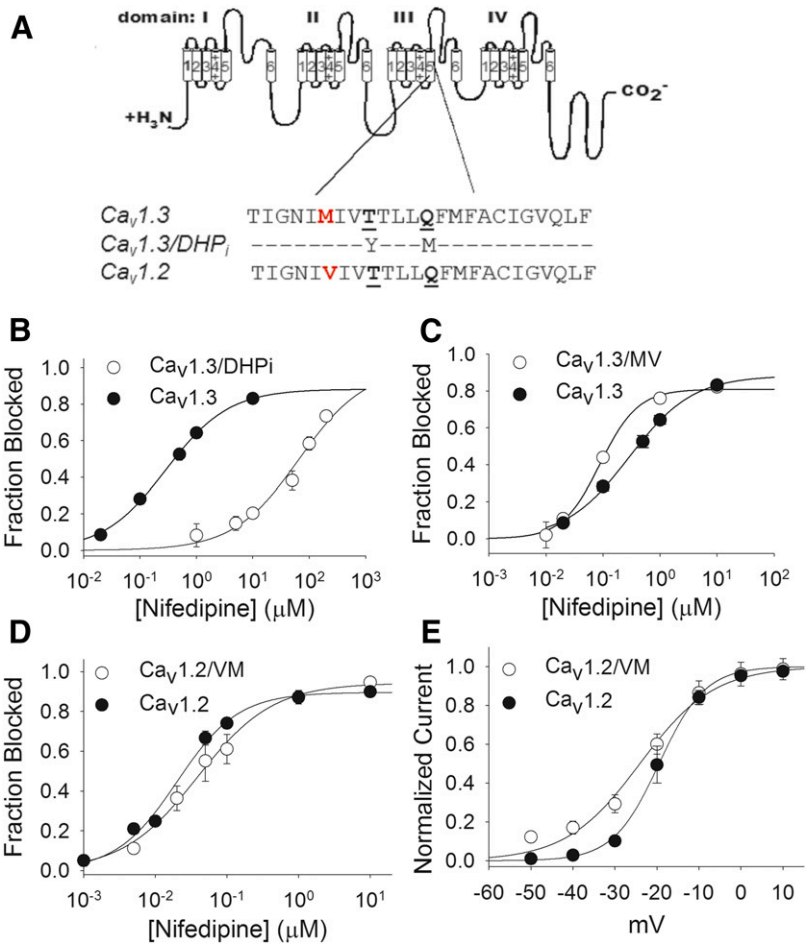

Fig. 2. Contribution of transmembrane domain IIIS5 to nifedipine block of $Ca_v1.3$. (A) Amino acid sequence alignment of the IIIS5 transmembrane domains in $Ca_v1.3$, $Ca_v1.2$, and the mutant $Ca_v1.3$/DHPi. The only difference is the M to V switch at position 1030/1036 (in red). The underlined residues were mutated to create $Ca_v1.3$/DHPi and are critical for dihydropyridine block of $Ca_v1.2$. (B) Nifedipine dose-response curve for block of $Ca_v1.3$/DHPi. The IC_{50} of nifedipine for $Ca_v1.3$/DHPi was estimated at ~93 μM. (C) Dose-response curve for nifedipine block of $Ca_v1.3$/MV. The IC_{50} value was 89 ± 7 nM (N = 5–7), less than the IC_{50} of nifedipine block of $Ca_v1.3$ ($P < 0.001$). (D) Dose-response curve for nifedipine block of $Ca_v1.2$/VM. The IC_{50} value was 39 ± 5 nM (N = 4–6), greater than the IC_{50} for block of $Ca_v1.2$ ($P < 0.05$). (E) Voltage-dependent activation of $Ca_v1.2$/VM. The $V_{1/2}$ activation for $Ca_v1.2$/VM was −24 ± 1 mV (N = 8), more negative than that for $Ca_v1.2$ ($P < 0.05$).

inactivation was not different from $Ca_v1.3$, and the voltage-dependence of activation was ~3 mV more negative than $Ca_v1.3$ (see Table 1). The IC_{50} for nifedipine block of $Ca_v1.3$/PEEP was 188 ± 28 nM, not statistically significantly lower than the IC_{50} for block of $Ca_v1.3$ (Fig. 3C; Table 1). However, the Hill slope for the dose-response curve for nifedipine block of $Ca_v1.3$PEEP (0.43 ± 0.02) was shallower than $Ca_v1.3$ ($P < 0.001$). We next turned our attention to a region of the IIIS5-3P loop proximal to IIIS5 that contains a cluster of three negatively charged residues in $Ca_v1.2$ (D1063, E1069, E1071), reported to affect DHP binding affinity (Wang et al., 2007). Only two of these negative charges are conserved in $Ca_v1.3$ (D1057 and E1065); moreover, the amino acid sequence surrounding these residues is highly divergent between $Ca_v1.2$ and $Ca_v1.3$ (see Fig. 3A). Therefore, we created the mutant $Ca_v1.3$/N6 with the $Ca_v1.2$ sequence from amino acid 1064–1070 (SSKQTEA) inserted into the corresponding position (1058–1064) in $Ca_v1.3$. We found that expression of $Ca_v1.3$/N6 yielded functional channels, but the current was outward with 180 mM NMDG in the intracellular solution and no NMDG in the extracellular solution. Therefore, we used NMDG-balanced solutions in recordings with $Ca_v1.3$/N6, which restored inward barium current. The voltage-dependence of activation of $Ca_v1.3$/N6 under these conditions was −17 ± 0.8 mV, and the voltage-dependence of inactivation was −34 ± 0.6 mV (Table 1). We found that the IC_{50} for nifedipine block of $Ca_v1.3$/N6 (116 ± 53 nM) was slightly ($P < 0.05$) lower than that for $Ca_v1.3$, but the Hill slope of the dose-response curve (0.52 ± 0.1) was also less than $Ca_v1.3$ ($P < 0.05$) (Fig. 3D).

Given that the decreases in nifedipine IC_{50} for both $Ca_v1.3$/MV and $Ca_v1.3$+ were relatively modest, we asked if combining these mutations would further increase the potency of nifedipine block. The $V_{1/2}$ activation of the resulting mutant channel, $Ca_v1.3$+V, was not different from $Ca_v1.3$, but the $V_{1/2}$ inactivation was shifted by −6 mV (see Table 1). However, the IC_{50} for nifedipine block of $Ca_v1.3$+V was reduced to 42 ± 5 nM (Fig. 3E), compared with 289 ± 30 nM for $Ca_v1.3$ ($P < 0.001$), but was still greater than the IC_{50} of nifedipine for $Ca_v1.2$ ($P < 0.05$). Thus, amino acid differences in the IIIS5-3P loop, along with the single amino acid divergence in IIIS5, account for the vast majority of the difference in potency of nifedipine block of $Ca_v1.2$ and $Ca_v1.3$.

We next asked if the small remaining gap in nifedipine potency between $Ca_v1.3$+V and $Ca_v1.2$ could be closed. Besides IIIS5 and the IIIS5-3P loop, transmembrane domain IIIS6 also contributes to the DHP binding pocket in $Ca_v1.2$ (Hockerman et al., 1997b). The only amino acid residue in IIIS6 not conserved between $Ca_v1.2$ and $Ca_v1.3$ is an I/V divergence at position 1156/1150; moreover, mutation of I1156 in $Ca_v1.2$ to A resulted in a significant decrease in DHP binding affinity (Peterson et al., 1997). Unfortunately, we found that substitution of V for I at position 1150 in IIIS6 of either $Ca_v1.3$+V or $Ca_v1.3$/MV resulted in channels that yielded little to no current upon expression in tsA201 cells.

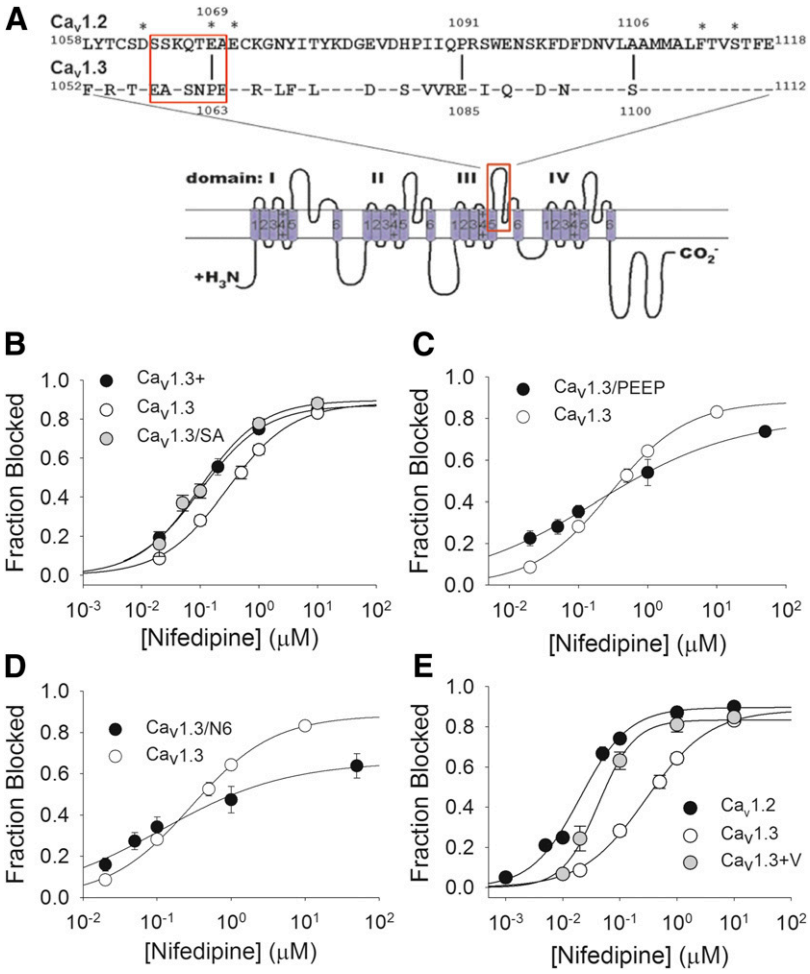

Fig. 3. Contribution of the IIIS5-3P loop to nifedipine block of $Ca_v1.3$. (A) Amino acid sequence alignment of the extracellular IIIS5-3P loops of $Ca_v1.2$ (aa 1058–1118) and $Ca_v1.3$ (aa 1052–1112). Twenty-four of the 60 amino acids in this segment are not conserved. Identities are indicated with a dash. Asterisks indicate amino acid residues previously reported to influence dihydropyridine modulation of $Ca_v1.2$. The $Ca_v1.3$+ mutant incorporated all of the $Ca_v1.2$-specific amino acids in this segment into $Ca_v1.3$. The $Ca_v1.3$ +V mutant is $Ca_v1.3$+ combined with the substitution of V for M at position 1030. The $Ca_v1.3$/SA mutant incorporated only the S to A substitution at position 1100. The $Ca_v1.3$/PEEP mutation incorporated the substitution of P for E and E for P at positions 1063 and 1085, respectively. The $Ca_v1.3$/N6 mutation incorporated the six $Ca_v1.2$-specific amino acid residues from position 1064 to 1070 (boxed residues) into $Ca_v1.3$. (B) Dose-response curve for block of $Ca_v1.3$+ and $Ca_v1.3$/SA by nifedipine. $Ca_v1.3$+ (black circles) and $Ca_v1.3$/SA (gray circles) were both more sensitive to block by nifedipine than $Ca_v1.3$ ($P < 0.001$; $P < 0.01$, respectively). IC_{50} for nifedipine block of: $Ca_v1.3$+ = 101 ± 4 nM (N = 6–8); $Ca_v1.3$/SA = 99 ± 24 nM (N = 4 to 5). (C) Dose-response curve for block of $Ca_v1.3$/PEEP by nifedipine. The IC_{50} for nifedipine block of $Ca_v1.3$/PEEP was 188 ± 28 nM (N = 3–7), not different from that of $Ca_v1.3$; however, the Hill slope (0.43 ± 0.02), was shallower than that for $Ca_v1.3$ (0.78 ± 0.04) ($P < 0.001$). (D) Dose-response curve for block of $Ca_v1.3$/N6 by nifedipine. The IC_{50} for nifedipine block of $Ca_v1.3$/N6 was 116 ± 53 nM (N = 5–9), lower than that of $Ca_v1.3$ ($P < 0.05$). The Hill slope was (0.52 ± 0.10), shallower than that for $Ca_v1.3$ (0.78 ± 0.04) ($P < 0.05$). (E) Dose-response curve for nifedipine block of $Ca_v1.3$+V compared with those for $Ca_v1.2$ and $Ca_v1.3$. The IC_{50} for nifedipine block of $Ca_v1.3$+V was 42 ± 5 nM (N = 4–10), lower than that for $Ca_v1.3$ ($P < 0.001$).

Differences in the IIIS5-3P Loop Are Responsible for the Difference in Potency of FPL in $Ca_v1.2$ and $Ca_v1.3$. The nondihydropyridine compound FPL 64176 (FPL) (Ginap et al., 1993) is a well characterized potentiator of $Ca_v1.2$ current (Liu et al., 2003). Reconstruction of the DHP binding site in the P/Q-type channel $Ca_v2.1$ conferred potentiation of current by FPL, as well as potent block by DHP antagonists (Sinnegger et al., 1997). However, very little is known about FPL modulation of $Ca_v1.3$. Therefore, we compared the potency of FPL potentiation of current in $Ca_v1.2$ and $Ca_v1.3$. The experiments with $Ca_v1.3$ used balanced NMDG solutions because we found that application of FPL frequently induced outward current when the extracellular solution contained no NMDG (Supplemental Fig. 3A), suggesting that FPL binding substantially affects the permeability of $Ca_v1.3$ to NMDG. We found that the EC_{50} for potentiation of current amplitude in $Ca_v1.2$ by FPL was 103 ± 40 nM (Fig. 4, A and D). In contrast, the EC_{50} for potentiation of $Ca_v1.3$ current amplitude by FPL was 854 ± 236 nM ($P < 0.05$) (Fig. 4, B and D). Thus, as with nifedipine, $Ca_v1.3$ is less sensitive to FPL than $Ca_v1.2$.

We next asked if some of the same differences between $Ca_v1.2$ and $Ca_v1.3$ that account for the difference in nifedipine potency could also account for the difference in the potency of FPL in these two channel subtypes. We first measured the potency of FPL potentiation of current in $Ca_v1.3$+V, since this mutant had nearly the same sensitivity to nifedipine as $Ca_v1.2$. We were able to perform these experiments in the standard solution set, since FPL did not induce outward current in $Ca_v1.3$+V. The EC_{50} for potentiation of current amplitude by FPL in $Ca_v1.3$+V was 99 ± 5 nM (Fig. 4, C and D), indistinguishable from the EC_{50} of FPL for potentiation of $Ca_v1.2$. We measured the EC_{50} for FPL potentiation of $Ca_v1.3$/MV current amplitude in the standard solution set since we did not observe outward currents in the presence of FPL in this mutant. The EC_{50} of FPL for $Ca_v1.3$/MV was 737 ± 20 nM, not different from the EC_{50} for $Ca_v1.3$ (Fig. 4D). Taken together, these results suggest that the molecular determinants of the difference in potency of FPL lie within the IIIS5-3P loop. $Ca_v1.3$+ exhibited outward current in the presence of FPL, similar to $Ca_v1.3$ (Supplemental Fig. 3A). However, we were unable to measure the potency of FPL potentiation of this mutant because, even in the NMDG-balanced solution set, FPL induced erratic changes in current amplitude (Supplemental Fig. 3B). We were able to measure the potency of FPL potentiation of the IIIS5-3P loop mutants $Ca_v1.3$/PEEP, $Ca_v1.3$/N6, and $Ca_v1.3$/SA, and found that none of these mutants displayed increased sensitivity to potentiation of current by FPL compared with $Ca_v1.3$ (Table 1). Thus, we have identified two regions of amino acid divergence between $Ca_v1.2$ and $Ca_v1.3$ within the IIIS5-3P loop, $Ca_v1.2$ 1106/$Ca_v1.3$ 1100 and $Ca_v1.2$ 1064–1070/$Ca_v1.3$ 1058–64, that

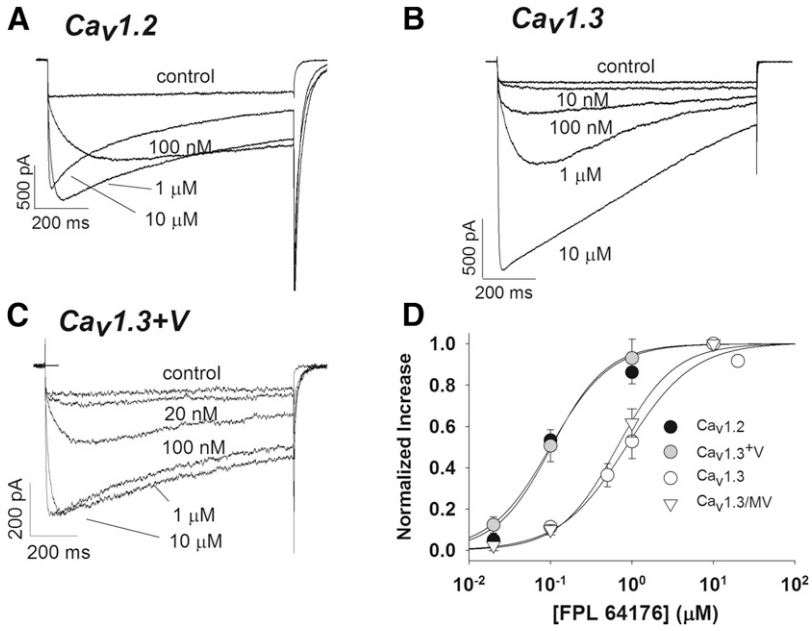

Fig. 4. Potency of FPL 64176 potentiation of $Ca_v1.2$, $Ca_v1.3$, and mutant channels. (A–C) Example traces showing FPL potentiation of $Ca_v1.2$, $Ca_v1.3$, and $Ca_v1.3$+V, respectively. Note the marked slowing of the tail current in $Ca_v1.2$ that is absent in $Ca_v1.3$. (D) Dose-response curves for FPL 64176 potentiation of $Ca_v1.2$, $Ca_v1.3$, and mutant channels. The EC_{50} values for FPL potentiation of current for $Ca_v1.2$ and $Ca_v1.3$ were 103 ± 40 nM (N = 3–8) and 854 ± 236 nM (N = 3–7), respectively ($P < 0.05$). The EC_{50} for FPL potentiation of the mutant $Ca_v1.3$+V (99 ± 5 nM) (N = 3–7) was not different from that of $Ca_v1.2$ but was different from that of $Ca_v1.3$ ($P < 0.05$). In contrast, the EC_{50} for FPL potentiation of the mutant $Ca_v1.3$/MV was 737 ± 20 nM (N = 5), not different from that of $Ca_v1.3$. Data are shown as the mean fractional increase in current compared with 10 μM FPL 64176 ± S.E.

appear to confer differences in sensitivity to nifedipine block but not in FPL potentiation of these two channels.

FPL has a strong effect on the kinetics of deactivation as well as the voltage-dependence of activation of $Ca_v1.2$ and $Ca_v1.3$. Figure 5 shows the effect of 10 μM FPL on tail-current kinetics, a measure of the rate of deactivation. $Ca_v1.3$ displays a fast rate of closing with a single time constant (τ) in the absence of FPL, but a second, slower τ is observed in the presence of FPL (Fig. 5A; Table 2). In contrast, deactivation in $Ca_v1.2$ in the absence of FPL follows two τs. However, a single slow τ is principally observed in the presence of FPL that is greater than both τs in the absence of FPL (Fig. 5B; Table 2).

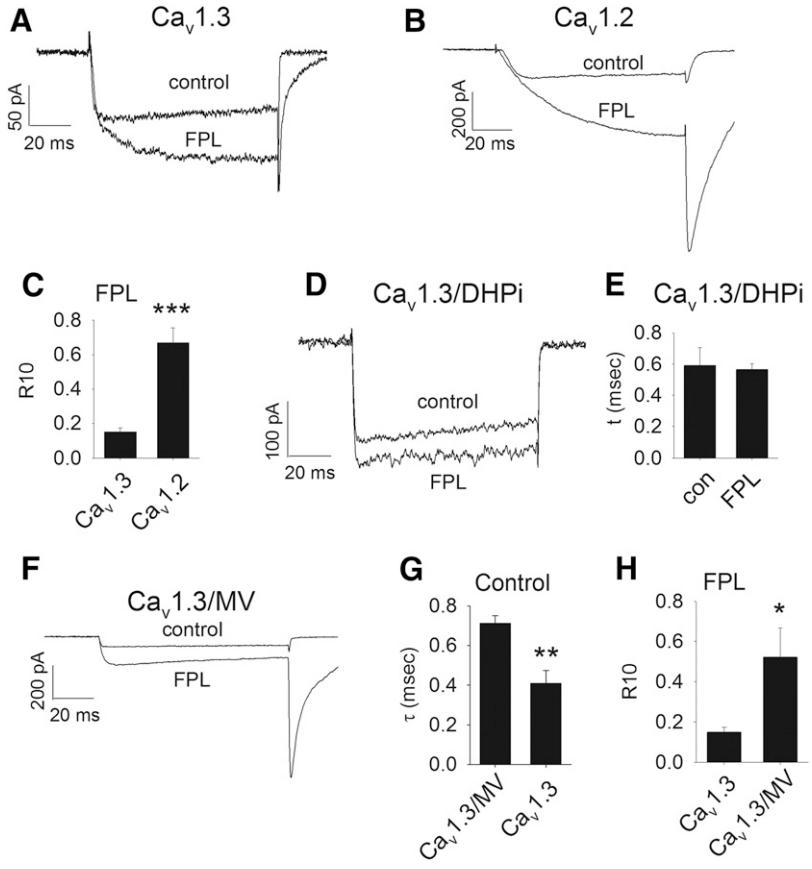

Fig. 5. Kinetics of tail-current decay in the presence and absence of FPL 64176 in $Ca_v1.2$, $Ca_v1.3$, and mutant channels. (A) Example 100-millisecond depolarization demonstrating tail-current decay in $Ca_v1.3$ in the presence or absence of 10 μM FPL 64176. (B) Example 100-millisecond depolarization demonstrating tail-current decay in $Ca_v1.2$ in the presence or absence of 10 μM FPL 64176. (C) The R10 value (fraction of tail current remaining 10 millisecond after peak) in the presence of FPL was greater in $Ca_v1.2$ (0.67 ± 0.09, N = 6) compared with that of $Ca_v1.3$ (0.15 ± 0.02) (N = 5) (***$P < 0.001$). (D) Example 100-millisecond depolarization demonstrating tail-current decay in $Ca_v1.3$/DHPi in the presence or absence of 10 μM FPL 64176. (E) The time constant for deactivation of $Ca_v1.3$/DHPi (τ = 0.59 ± 0.11 milliseconds, N = 5) was not affected by the presence of 10 μM FPL (τ = 0.60 ± 0.04 milliseconds, N = 5). (F) Example 100-millisecond depolarization demonstrating tail-current decay in $Ca_v1.3$/MV in the presence or absence of 10 μM FPL 64176. (G) The time constant for deactivation of $Ca_v1.3$/MV in the absence of FPL followed a single time constant (τ = 0.70 ± 0.13 milliseconds, N = 5) that was slower than that of $Ca_v1.3$ (**$P < 0.01$). (H) The R10 value for $Ca_v1.3$/MV tail current in the presence of 10 μM FPL (0.51 ± 0.15, N = 5) was greater than that of $Ca_v1.3$ (*$P < 0.05$).

TABLE 2
Kinetics of tail current decay in the presence and absence of FPL 64176

Channel	Frac. Fast	τ-Fast (ms)	Frac Slow	τ-Slow	Frac Slow FPL	τ-FPL	FPL R10	N
				ms		*ms*		
$Ca_v1.2$	0.79 ± 0.08	0.37 ± 0.05	0.18 ± 0.08	6.5 ± 0.6	0.64 ± 0.20	24 ± 7$^{\#}$	0.67 ± 0.09***	6
$Ca_v1.3$	0.96 ± 0.01	0.41 ± 0.07	NA	NA	0.34 ± 0.06	11 ± 1$^{\#\#\#}$	0.15 ± 0.02	5
$Ca_v1.3$/DHPi	0.94 ± 0.02	0.59 ± 0.11	NA	NA	NA	0.60 ± 0.04	ND	5
$Ca_v1.3$+V	0.96 ± 0.01	0.70 ± 0.13	NA	NA	0.84 ± 0.05	6.0 ± 1$^{\#\#}$	0.39 ± 0.07*	6
$Ca_v1.3$/MV	0.97 ± 0.01	0.71 ± 0.04*	NA	NA	0.53 ± 0.13	39 ± 9$^{\#}$	0.52 ± 0.15*	5
$Ca_v1.2$/VM	0.96 ± 0.04	0.68 ± 0.15	NA	NA	0.73 ± 0.10	29 ± 7$^{\#\#}$	0.71 ± 0.08***	6
$Ca_v1.3$/PEEP	0.96 ± 0.02	0.77 ± 0.08**	NA	NA	0.71 ± 0.18	12 ± 3$^{\#\#}$	0.34 ± 0.11	5

*$P < 0.05$; **$P < 0.01$; ***$P < 0.001$ compared with $Ca_v1.3$.
$^{\#}P < 0.05$; $^{\#\#}P < 0.01$; $^{\#\#\#}P < 0.001$ compared with absence of FPL.

Given the differences in the kinetics of deactivation in $Ca_v1.3$ versus $Ca_v1.2$, we compared the FPL-induced slowing of deactivation in these channels by measuring the fraction of the tail current remaining 10 milliseconds after reaching peak (R10). The R10 for both $Ca_v1.2$ and $Ca_v1.3$ in the absence of FPL was negligible. Figure 5C shows that the R10 of $Ca_v1.2$ in the presence of 10 μM FPL (0.67 ± 0.09) was greater than that of $Ca_v1.3$ (0.15 ± 0.02) ($P < 0.001$), indicating a greater slowing of deactivation by FPL in $Ca_v1.2$. We also found that FPL shifted the $V_{1/2}$ activation of $Ca_v1.2$ by −26 mV but only −10 mV in $Ca_v1.3$ (Table 2). Thus, FPL is not only more potent in stimulating current amplitude in $Ca_v1.2$ compared with $Ca_v1.3$ but also has stronger effects on deactivation kinetics and the voltage-dependence of activation in $Ca_v1.2$ at a maximally effective concentration (10 μM).

We next asked if the $Ca_v1.3$/DHPi channel was less sensitive to FPL than $Ca_v1.3$. Deactivation of $Ca_v1.3$/DHPi followed a single τ that was not different from that of $Ca_v1.3$ (Table 2) but was not altered by 10 μM FPL (Fig. 5, D and E). Not surprisingly, no significant increase in current was observed upon application of 10 μM FPL to $Ca_v1.3$DHPi. Interestingly, 10 μM FPL did shift the $V_{1/2}$ activation of $Ca_v1.3$DHPi by −9 mV (Table 2). Since IIIS5 is clearly crucial for the action of FPL, we examined the kinetics of deactivation in $Ca_v1.3$/MV (Fig. 5F). In the absence of FPL, $Ca_v1.3$/MV deactivation followed a single τ (0.71 ± 0.04 milliseconds) that was slightly, but statistically significantly greater than $Ca_v1.3$ (0.41 ± 0.07 milliseconds) ($P < 0.01$) (Fig. 5G). In the presence of 10 μM FPL, the R10 was greater in $Ca_v1.3$/MV (0.52 ± 0.15 milliseconds) ($P < 0.05$) compared with $Ca_v1.3$ (Fig. 5H). However, deactivation of $Ca_v1.2$/VM was not different from that of $Ca_v1.2$ either in the absence or presence of FPL (Table 2). Thus, the M to V switch at position 1030 of $Ca_v1.3$ does not affect FPL potency but does affect both deactivation and slowing of deactivation by FPL.

Discussion

The voltage-dependence and sensitivity to nimodipine (a DHP antagonist) of the $Ca_v1.3$ cDNA used in this study ($Ca_v1.3_{42}$) was previously characterized (Xu and Lipscombe, 2001). The $V_{1/2}$ activation reported here is indistinguishable from that initial characterization. Further, Xu and Lipscombe reported an ~20-fold higher IC_{50} for nimodipine block of $Ca_v1.3$ compared with $Ca_v1.2$. For our comparison of DHP antagonist potency, we chose nifedipine since it is the most compact molecule in this class, with no extended side chains that might interact with amino acids outside of the canonical DHP binding site, yet it retains excellent potency. Our results indicating an ~13-fold higher IC_{50} for nifedipine block of $Ca_v1.3$ compared with $Ca_v1.2$ is in line with the decreased potency of nimodipine in block of $Ca_v1.3$ compared with $Ca_v1.2$ reported by Xu and Lipscombe. Though they did not report an EC_{50} for agonist potentiation of $Ca_v1.3$, Xu and Lipscombe did report a modest shift in $V_{1/2}$ activation of $Ca_v1.3$ by 1 μM concentration of DHP agonist Bay K 8644 (~ −7 mV), similar to the modest leftward shift in $V_{1/2}$ activation we observed in $Ca_v1.3$ in the presence of 10 μM FPL. Thus, our data show that our expression system recapitulates the primary differences between $Ca_v1.2$ and $Ca_v1.3$, most notably, the left-shifted activation and lower sensitivity of current to block by DHP antagonists of $Ca_v1.3$ compared with $Ca_v1.2$.

Another study examined both the binding affinity and block potency of the DHP antagonist PN200-110 (isradipine) for a $Ca_v1.3$ clone from human pancreas ($Ca_v1.3_{8A}$) (Koschak et al., 2001). Interestingly, the K_D for [^{3}H]PN200-110 binding was not significantly different between $Ca_v1.3_{8A}$ and $Ca_v1.2$ cloned from rabbit cardiac muscle (Tanabe et al., 1987). However, the IC_{50} for block of current by PN200-110 was reported to be 8.5-fold higher for $Ca_v1.3_{8A}$ than $Ca_v1.2$, in excellent agreement with the difference in nifedipine potency in blocking $Ca_v1.3$ and $Ca_v1.2$ in this study. K_D values for binding of DHPs to L-type channels in isolated membranes are invariably lower than IC_{50} values for current block. For example, the K_D for binding of [^{3}H]PN200-110 to the $Ca_v1.2$ clone used in this study is 55 pM, whereas the IC_{50} for PN200-110 block is 7 nM (Peterson et al., 1997). Binding isotherms in both studies clearly indicated a single [^{3}H]PN200-110 binding site, which probably reflects the open, inactivated state of the channel at 0 mV. Thus, it is probable that the Hill slopes different from 1 that we observed for nifedipine block of $Ca_v1.3$ and some of the mutant channels used in this study reflect the presence of distinct voltage-dependent channel conformations that regulate DHP affinity.

Though the DHP binding pockets of $Ca_v1.2$ and $Ca_v1.3$ are highly conserved, our results suggest that relatively minor differences in transmembrane segment IIIS5 and the IIIS5-3P loop can largely account for the difference in potency of nifedipine in block of $Ca_v1.2$ and $Ca_v1.3$. The IIIS5 helix is clearly a critical component of the $Ca_v1.3$ DHP binding pocket, as mutation of T1033 and Q1037 in $Ca_v1.3$/DHPi results in a marked loss of nifedipine potency. The side chains of M1030/V1036 in $Ca_v1.3$ and $Ca_v1.2$ are projected to align to the same face of the IIIS5 helix as the T and Q residues required for high-potency DHP block (Mitterdorfer et al., 1996), supporting our finding that swapping the $Ca_v1.3$-specific residue at

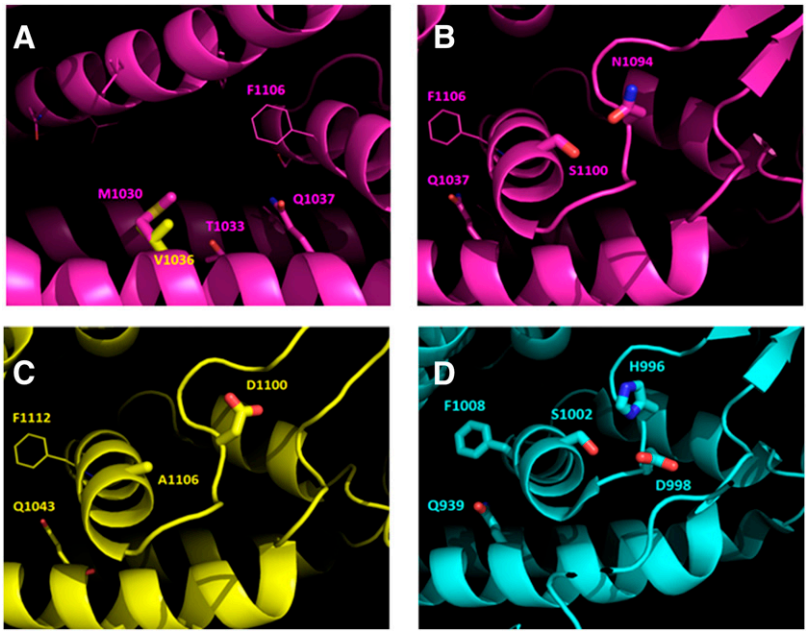

Fig. 6. Influence of $Ca_v1.3$-specific amino acid residues on the DHP binding pocket. Homology models of $Ca_v1.2$ and $Ca_v1.3$ were created on the basis of the high-resolution cryoEM structure of $Ca_v1.1$. (A) View of the DHP binding pocket of $Ca_v1.3$ framed by the IIIS5 helix (bottom), IVS6 helix (top), and the 3P helix (right) with V1036 from $Ca_v1.2$ superimposed on M1030. (B) View of the backside of the 3P helix in $Ca_v1.3$ showing a potential H-bond between the $Ca_v1.3$-specific residues S1100 and N1094. (C) View of the backside of the 3P helix in $Ca_v1.2$ with the positions of A1106 and D1100 indicated. (D) View of the backside of the 3P helix in $Ca_v1.1$ showing potential H-bond between S1002 and H996 facilitated by D998.

this position into $Ca_v1.2$ (V1036M) shifts nifedipine potency toward that of $Ca_v1.3$, and vice versa. Interestingly, the swap of channel subtype-specific residues in this position also results in small reciprocal shifts in $V_{1/2}$ activation (Table 1). However, only the $Ca_v1.3$/MV mutant exhibited slower deactivation, both in the presence and absence of FPL (Table 2). This observation, that decreasing the bulk of the amino acid side-chain at position 1030 in $Ca_v1.3$ affects voltage-dependence of activation and the rate of tail-current decay, suggests that position 1030 in IIIS5 (outer pore helix) may interact with IIIS6 (inner pore helix) in a manner that regulates channel gating. Previously published models of DHP binding in $Ca_v1.2$ suggest that amino acid residues directly interacting with DHP drugs are conserved between $Ca_v1.2$ and $Ca_v1.3$ (Cosconati et al., 2007; Tikhonov and Zhorov, 2009). To understand how subtle differences in amino acid sequence might account for a significant difference in nifedipine potency, we constructed homology models of $Ca_v1.3$ and $Ca_v1.2$ (Fig. 6) on the basis of the recently published high-resolution cryo-EM structure of $Ca_v1.1$ (Wu et al., 2016). The models suggest that the increase in side-chain bulk between $Ca_v1.3$ and $Ca_v1.2$ at position 1030/1036 (M vs. V) could potentially decrease accessibility of nifedipine to the critical Q1037 and F1106 residues (Fig. 6A). In addition, the model predicts that S1100 in $Ca_v1.3$ can form a hydrogen bond with N1094, an interaction that could potentially constrain the movement of the 3P helix during nifedipine binding (Fig. 6B). The corresponding positions in $Ca_v1.2$ are occupied by an alanine residue (1106) and a glutamate (1100), precluding such an interaction (Fig. 6C). Interestingly, S1100 of $Ca_v1.3$ is conserved in the corresponding position of $Ca_v1.1$ (S1002) and the position corresponding to N1094 of $Ca_v1.3$ is a histidine in $Ca_v1.1$ (H996). These residues, with the assistance of D998, may form a hydrogen bond in $Ca_v1.1$ (Fig. 6D), which may contribute to the lower binding affinity of $Ca_v1.1$ for [^{3}H]PN200-110 (270 pM) (Peterson et al., 1996) compared with $Ca_v1.2$ (55 pM) (Peterson et al., 1997). Thus, our model suggests that the effect of the $Ca_v1.3$S/A mutation on nifedipine potency is indirect, and that the displacement of the 3P helix may be required for high potency block of $Ca_v1.2$ by DHP drugs.

Our studies of FPL potentiation of $Ca_v1.2$, $Ca_v1.3$, and the various mutant channels also yielded some novel results. First, Fig. 4 clearly shows that FPL is much more potent in potentiating current conducted by $Ca_v1.2$ compared with $Ca_v1.3$. This difference can be ascribed completely to amino acid differences in the IIIS5-3P loop between these two channels. Nevertheless, the conserved T and Q residues in IIIS5 are clearly important for FPL action on $Ca_v1.3$ even though the nearby M1030V mutation did not increase the potency of FPL action in isolation. However, the inclusion of V1030 in $Ca_v1.3$+V was critical for stabilizing FPL potentiation of current and revealing the increased sensitivity of this mutant to FPL. Interestingly, despite a complete loss of slowing of deactivation by FPL, the FPL-induced shift in $V_{1/2}$ activation in $Ca_v1.3$/DHPi was not different from that of $Ca_v1.3$, suggesting distinct sites of action on $Ca_v1.3$ for these two characteristic effects of FPL on L-type channel gating. Unfortunately, we were not able to further resolve the amino acid resides that confer the difference in sensitivity to FPL between $Ca_v1.2$ and $Ca_v1.3$ beyond the IIIS5-3P loop, as none of the mutations within this domain that increased nifedipine potency improved FPL potency at $Ca_v1.3$. It is possible that these determinants may be among the sixteen other amino acid differences between $Ca_v1.2$ and $Ca_v1.3$ within this domain that we did not examine.

In our studies of the $Ca_v1.3$/N6 mutant, we made the unexpected observation that outward current often developed during the course of an experiment. The standard solution set used in this study sets up a large NMDG gradient across the membrane. Mutations in the pore region of $Ca_v1.2$ were previously reported to lead to enhanced permeability of NMDG, as evidenced by a marked shift in reversal potential that was abolished by equalizing the NMDG concentration in the extracellular and intracellular solutions (Hockerman

et al., 1995). Indeed, we found that, by equalizing the NMDG concentration in the intra- and extracellular solutions, the outward current observed in the $Ca_v1.3$/N6 mutant was abolished, and we were able to complete the biophysical and pharmacological measurements reported in Table 1. Likewise, we found that $Ca_v1.3$ and the $Ca_v1.3+$ mutant tended to undergo current reversal upon FPL application (Supplemental Fig. 3A) that was abolished in $Ca_v1.3$ by equalizing the NMDG concentrations. However, even this maneuver left unstable current when FPL was applied to $Ca_v1.3+$, and we were unable to determine an EC_{50} for FPL stimulation of this mutant (Supplemental Fig. 3B). FPL was previously reported to alter the permeability of $Ca_v1.2$ (Fan et al., 2001), such that Cd^{2+} became a permeant ion, rather than a pore blocker, in the absence of Ca^{2+}. Thus, our observation that FPL can induce NMDG permeability in $Ca_v1.3$ is consistent with the notion that FPL binding may induce conformational changes in the IIIS5-3P loop that affect the ion selectivity of $Ca_v1.3$. Interestingly, neither the $Ca_v1.3+V$ nor the $Ca_v1.3M/V$ mutant conducted outward current in the presence of FPL in the standard solution set, suggesting that the M1030 residue may play a role in the observed permeability changes in $Ca_v1.3$.

In summary, this study demonstrates that the reduced sensitivity of $Ca_v1.3$ to both nifedipine and FPL compared with $Ca_v1.2$ can be attributed largely to amino acid differences within the previously defined DHP binding pocket. In the case of nifedipine, this difference can be attributed to the M/V divergence in transmembrane domain IIIS5, and an S/A divergence in the IIIS5-3P loop. Our homology models suggest that divergence in IIIS5 results in distinct stearic effects on drug binding, whereas the divergence in the IIIS5-3P loop may regulate displacement of the 3P helix upon ligand binding.

Acknowledgments

We gratefully acknowledge Dr. Terrance Snutch (University of British Columbia) and Dr. Tuck-Wah Soong (National University of Singapore) for generously providing cDNAs encoding $Ca_v1.2$ and $Ca_v1.3$ subunits, respectively.

Authorship Contributions

Participated in research design: Wang, Hockerman.

Conducted experiments: Wang, Tang, Harvey, Hockerman.

Contributed new reagents or analytic tools: Salyer, Li, Rantz, Lill.

Performed data analysis: Wang, Tang, Harvey, Hockerman.

Wrote or contributed to the writing of the manuscript: Wang, Hockerman.

References

Bason C, Lorini R, Lunardi C, Dolcino M, Giannattasio A, d'Annunzio G, Rigo A, Pedemonte N, Corrocher R, and Puccetti A (2013) In type 1 diabetes a subset of anti-coxsackievirus B4 antibodies recognize autoantigens and induce apoptosis of pancreatic beta cells. *PLoS One* **8**:e57729.

Benkert P, Biasini M, and Schwede T (2011) Toward the estimation of the absolute quality of individual protein structure models. *Bioinformatics* **27**:343–350.

Bertoni M, Kiefer F, Biasini M, Bordoli L, and Schwede T (2017) Modeling protein quaternary structure of homo- and hetero-oligomers beyond binary interactions by homology. *Sci Rep* **7**:10480.

Bienert S, Waterhouse A, de Beer TA, Tauriello G, Studer G, Bordoli L, and Schwede T (2017) The SWISS-MODEL repository-new features and functionality. *Nucleic Acids Res* **45**(D1):D313–D319.

Castellano A, Wei X, Birnbaumer L, and Perez-Reyes E (1993) Cloning and expression of a third calcium channel beta subunit. *J Biol Chem* **268**:3450–3455.

Catterall WA (2000) Structure and regulation of voltage-gated Ca^{2+} channels. *Annu Rev Cell Dev Biol* **16**:521–555.

Chang CC, Cao S, Kang S, Kai L, Tian X, Pandey P, Dunne SF, Luan CH, Surmeier DJ, and Silverman RB (2010) Antagonism of 4-substituted 1,4-dihydropyridine-3,5-dicarboxylates toward voltage-dependent L-type Ca^{2+} channels Ca_V 1.3 and Ca_V 1.2. *Bioorg Med Chem* **18**:3147–3158.

Cheng RC, Tikhonov DB, and Zhorov BS (2009) Structural model for phenylalkylamine binding to L-type calcium channels. *J Biol Chem* **284**:28332–28342.

Cosconati S, Marinelli L, Lavecchia A, and Novellino E (2007) Characterizing the 1,4-dihydropyridines binding interactions in the L-type Ca^{2+} channel: model construction and docking calculations. *J Med Chem* **50**:1504–1513.

Dilmac N, Hilliard N, and Hockerman GH (2003) Molecular determinants of Ca^{2+} potentiation of diltiazem block and Ca^{2+}-dependent inactivation in the pore region of $ca_v1.2$. *Mol Pharmacol* **64**:491–501.

Dilmac N, Hilliard N, and Hockerman GH (2004) Molecular determinants of frequency dependence and Ca^{2+} potentiation of verapamil block in the pore region of $Ca_v1.2$. *Mol Pharmacol* **66**:1236–1247.

Fan J, Yuan Y, and Palade P (2001) FPL-64176 modifies pore properties of L-type $Ca^{(2+)}$ channels. *Am J Physiol Cell Physiol* **280**:C565–C572.

Ginap T, Dooley DJ, and Feuerstein TJ (1993) The non-dihydropyridine L-type voltage-sensitive calcium channel activator FPL 64176 enhances $K^{(+)}$-evoked efflux of [^{3}H]norepinephrine from rat neocortical slices. *Neurosci Lett* **156**:35–38.

Guex N, Peitsch MC, and Schwede T (2009) Automated comparative protein structure modeling with SWISS-MODEL and Swiss-PdbViewer: a historical perspective. *Electrophoresis* **30** (Suppl 1):S162–S173.

Guzman JN, Sánchez-Padilla J, Chan CS, and Surmeier DJ (2009) Robust pacemaking in substantia nigra dopaminergic neurons. *J Neurosci* **29**:11011–11019.

Guzman JN, Sanchez-Padilla J, Wokosin D, Kondapalli J, Ilijic E, Schumacker PT, and Surmeier DJ (2010) Oxidant stress evoked by pacemaking in dopaminergic neurons is attenuated by DJ-1. *Nature* **468**:696–700.

Hell JW, Westenbroek RE, Warner C, Ahlijanian MK, Prystay W, Gilbert MM, Snutch TP, and Catterall WA (1993) Identification and differential subcellular localization of the neuronal class C and class D L-type calcium channel alpha 1 subunits. *J Cell Biol* **123**:949–962.

Hering S, Aczél S, Grabner M, Döring F, Berjukow S, Mitterdorfer J, Sinnegger MJ, Striessnig J, Degtiar VE, Wang Z, et al. (1996) Transfer of high sensitivity for benzothiazepines from L-type to class A (BI) calcium channels. *J Biol Chem* **271**: 24471–24475.

Hockerman GH, Dilmac N, Scheuer T, and Catterall WA (2000) Molecular determinants of diltiazem block in domains IIIS6 and IVS6 of L-type $Ca^{(2+)}$ channels. *Mol Pharmacol* **58**:1264–1270.

Hockerman GH, Johnson BD, Abbott MR, Scheuer T, and Catterall WA (1997a) Molecular determinants of high affinity phenylalkylamine block of L-type calcium channels in transmembrane segment IIIS6 and the pore region of the alpha1 subunit. *J Biol Chem* **272**:18759–18765.

Hockerman GH, Johnson BD, Scheuer T, and Catterall WA (1995) Molecular determinants of high affinity phenylalkylamine block of L-type calcium channels. *J Biol Chem* **270**:22119–22122.

Hockerman GH, Peterson BZ, Johnson BD, and Catterall WA (1997b) Molecular determinants of drug binding and action on L-type calcium channels. *Annu Rev Pharmacol Toxicol* **37**:361–396.

Hockerman GH, Peterson BZ, Sharp E, Tanada TN, Scheuer T, and Catterall WA (1997c) Construction of a high-affinity receptor site for dihydropyridine agonists and antagonists by single amino acid substitutions in a non-L-type Ca2+ channel. *Proc Natl Acad Sci USA* **94**:14906–14911.

Huang H, Ng CY, Yu D, Zhai J, Lam Y, and Soong TW (2014) Modest CaV1.342-selective inhibition by compound 8 is β-subunit dependent. *Nat Commun* **5**:4481.

Huang H, Yu D, and Soong TW (2013) C-terminal alternative splicing of $Ca_V1.3$ channels distinctively modulates their dihydropyridine sensitivity. *Mol Pharmacol* **84**:643–653.

Juntti-Berggren L, Larsson O, Rorsman P, Ammälä C, Bokvist K, Wåhlander K, Nicotera P, Dypbukt J, Orrenius S, Hallberg A, et al. (1993) Increased activity of L-type Ca^{2+} channels exposed to serum from patients with type I diabetes. *Science* **261**:86–90.

Kang S, Cooper G, Dunne SF, Dusel B, Luan CH, Surmeier DJ, and Silverman RB (2012) $Ca_V1.3$-selective L-type calcium channel antagonists as potential new therapeutics for Parkinson's disease. *Nat Commun* **3**:1146.

Kang S, Cooper G, Dunne SF, Luan CH, Surmeier DJ, and Silverman RB (2013) Structure-activity relationship of N,N′-disubstituted pyrimidinetriones as $Ca_{(V)}1.3$ calcium channel-selective antagonists for Parkinson's disease. *J Med Chem* **56**: 4786–4797.

Koschak A, Reimer D, Huber I, Grabner M, Glossmann H, Engel J, and Striessnig J (2001) Alpha 1D ($Ca_v1.3$) subunits can form l-type Ca^{2+} channels activating at negative voltages. *J Biol Chem* **276**:22100–22106.

Lin M, Aladejebi O, and Hockerman GH (2011) Distinct properties of amlodipine and nicardipine block of the voltage-dependent Ca^{2+} channels $Ca_v1.2$ and $Ca_v2.1$ and the mutant channels $Ca_v1.2$/dihydropyridine insensitive and $Ca_v2.1$/dihydropyridine sensitive. *Eur J Pharmacol* **670**:105–113.

Liu L, Gonzalez PK, Barrett CF, and Rittenhouse AR (2003) The calcium channel ligand FPL 64176 enhances L-type but inhibits N-type neuronal calcium currents. *Neuropharmacology* **45**:281–292.

Mitterdorfer J, Wang Z, Sinnegger MJ, Hering S, Striessnig J, Grabner M, and Glossmann H (1996) Two amino acid residues in the IIIS5 segment of L-type calcium channels differentially contribute to 1,4-dihydropyridine sensitivity. *J Biol Chem* **271**:30330–30335.

Ortner NJ, Bock G, Vandael DH, Mauersberger R, Draheim HJ, Gust R, Carbone E, Tuluc P, and Striessnig J (2014) Pyrimidine-2,4,6-triones are a new class of voltage-gated L-type Ca^{2+} channel activators. *Nat Commun* **5**:3897.

Peterson BZ, Johnson BD, Hockerman GH, Acheson M, Scheuer T, and Catterall WA (1997) Analysis of the dihydropyridine receptor site of L-type calcium channels by alanine-scanning mutagenesis. *J Biol Chem* **272**:18752–18758.

Peterson BZ, Tanada TN, and Catterall WA (1996) Molecular determinants of high affinity dihydropyridine binding in L-type calcium channels. *J Biol Chem* **271**:5293–5296.

Platzer J, Engel J, Schrott-Fischer A, Stephan K, Bova S, Chen H, Zheng H, and Striessnig J (2000) Congenital deafness and sinoatrial node dysfunction in mice lacking class D L-type Ca^{2+} channels. *Cell* **102**:89–97.

Ran Y, He Y, Yang G, Johnson JL, and Yalkowsky SH (2002) Estimation of aqueous solubility of organic compounds by using the general solubility equation. *Chemosphere* **48**:487–509.
Seino S, Chen L, Seino M, Blondel O, Takeda J, Johnson JH, and Bell GI (1992) Cloning of the alpha 1 subunit of a voltage-dependent calcium channel expressed in pancreatic beta cells. *Proc Natl Acad Sci USA* **89**:584–588.
Sinnegger MJ, Wang Z, Grabner M, Hering S, Striessnig J, Glossmann H, and Mitterdorfer J (1997) Nine L-type amino acid residues confer full 1,4-dihydropyridine sensitivity to the neuronal calcium channel alpha1A subunit. Role of L-type Met1188. *J Biol Chem* **272**:27686–27693.
Snutch TP, Tomlinson WJ, Leonard JP, and Gilbert MM (1991) Distinct calcium channels are generated by alternative splicing and are differentially expressed in the mammalian CNS. *Neuron* **7**:45–57.
Surmeier DJ and Schumacker PT (2013) Calcium, bioenergetics, and neuronal vulnerability in Parkinson's disease. *J Biol Chem* **288**:10736–10741.
Tanabe T, Takeshima H, Mikami A, Flockerzi V, Takahashi H, Kangawa K, Kojima M, Matsuo H, Hirose T, and Numa S (1987) Primary structure of the receptor for calcium channel blockers from skeletal muscle. *Nature* **328**:313–318.
Tenti G, Parada E, León R, Egea J, Martínez-Revelles S, Briones AM, Sridharan V, López MG, Ramos MT, and Menéndez JC (2014) New 5-unsubstituted dihydropyridines with improved $Ca_V1.3$ selectivity as potential neuroprotective agents against ischemic injury. *J Med Chem* **57**:4313–4323.
Tikhonov DB and Zhorov BS (2009) Structural model for dihydropyridine binding to L-type calcium channels. *J Biol Chem* **284**:19006–19017.
Wang X, Du L, and Peterson BZ (2007) Calcicludine binding to the outer pore of L-type calcium channels is allosterically coupled to dihydropyridine binding. *Biochemistry* **46**:7590–7598.
Waterhouse A, Bertoni M, Bienert S, Studer G, Tauriello G, Gumienny R, Heer FT, de Beer TAP, Rempfer C, Bordoli L, et al. (2018) SWISS-MODEL: homology modelling of protein structures and complexes. *Nucleic Acids Res* **46**:W296–W303.
Williams ME, Feldman DH, McCue AF, Brenner R, Velicelebi G, Ellis SB, and Harpold MM (1992) Structure and functional expression of alpha 1, alpha 2, and beta subunits of a novel human neuronal calcium channel subtype. *Neuron* **8**:71–84.
Wu J, Yan Z, Li Z, Qian X, Lu S, Dong M, Zhou Q, and Yan N (2016) Structure of the voltage-gated calcium channel $Ca_{(v)}1.1$ at 3.6 Å resolution. *Nature* **537**:191–196.
Xu W and Lipscombe D (2001) Neuronal $Ca_{(V)}1.3$alpha(1) L-type channels activate at relatively hyperpolarized membrane potentials and are incompletely inhibited by dihydropyridines. *J Neurosci* **21**:5944–5951.
Yamaguchi S, Okamura Y, Nagao T, and Adachi-Akahane S (2000) Serine residue in the IIIS5-S6 linker of the L-type Ca^{2+} channel alpha 1C subunit is the critical determinant of the action of dihydropyridine Ca^{2+} channel agonists. *J Biol Chem* **275**:41504–41511.
Yamaguchi S, Zhorov BS, Yoshioka K, Nagao T, Ichijo H, and Adachi-Akahane S (2003) Key roles of Phe1112 and Ser1115 in the pore-forming IIIS5-S6 linker of L-type Ca^{2+} channel alpha1C subunit (Ca_V 1.2) in binding of dihydropyridines and action of Ca^{2+} channel agonists. *Mol Pharmacol* **64**:235–248.
Yang J, Ellinor PT, Sather WA, Zhang JF, and Tsien RW (1993) Molecular determinants of Ca^{2+} selectivity and ion permeation in L-type Ca^{2+} channels. *Nature* **366**:158–161.

Address correspondence to: Dr. Gregory H. Hockerman, Purdue University, 575 Stadium Mall Drive, West Lafayette, IN 47907-2091. E-mail: gregh@purdue.edu